Supporting Information

Efficient $NiCoSe_4$/NiCo-LDH/CF catalyst for the co-production of value-added formate and hydrogen via selective methanol electro-oxidation

Jiaxin Li, Hongmei Yu*, Jun Chi, Xu Luo, Tongzhou Li, Zhigang Shao

Fuel Cell System and Engineering Laboratory, Dalian Institute of Chemical Physics, Chinese Academy of Sciences, Dalian 116023, Liaoning, China

*Corresponding author.

E-mail addresses: hmyu@dicp.ac.cn

Experiments

1. Materials and chemicals

The cobalt foam (CF, thickness of 1.0 mm) was purchased from Willtek Photoelectric Materials Co., Ltd. (Suzhou China). Nickel nitrate hexahydrate ($Ni(NO_3)_2·6H_2O$, ≥98%), hydrochloric acid (HCl, 36-38%), absolute alcohol (C_2H_5OH), and acetone (C_3H_6O) were purchased from Damao Co., Ltd. (Tianjin China). Cobalt nitrate hexahydrate ($Co(NO_3)_2·6H_2O$, ≥99%), ammonium fluoride (NH_4F, ≥96%), urea ($CO(NH_2)_2$, ≥99%), selenium powder (Se, ≥99.9%), methanol (CH_3OH, ≥99.9%), and formate (CH_2O_2, ≥98%) were purchased from Aladdin Reagent Co., Ltd. (Shanghai China). Potassium hydroxide (KOH, ≥95%) was purchased from Macklin Reagent Co., Ltd. (Shanghai China). All the chemicals were used as received without any further purification. Ultrapure water with a resistance of 18.2 MΩ (ELix advantage) was used throughout all experiments.

2. Electrochemical measurements

The electrochemical data was acquired by the Gamry Interface 5000E and processed through the Echem Analyst software package. The working electrode was the as-prepared self-supported electrode. Its exposed geometric area was strictly fixed at 1 cm^2 with a platinum clip. A graphite rod and a saturated calomel electrode (SCE) were employed as counter and reference electrodes, respectively. The accuracy of the reference electrode was carefully checked before and after the tests to ensure precise measurements. All the potentials were converted and referred to the reversible hydrogen electrode (RHE) unless otherwise noted, E (RHE) = E (SCE) + 0.0591*pH + 0.24 V. The current density was reported by normalizing the current to the geometric surface area of the electrode unless otherwise noted.

The SMOR measurements were tested in a typical three-electrode system. The catalytic activity was evaluated by cyclic voltammetry (CV) with the potential range from 1.03 V to 1.73 V vs. RHE in 1 M KOH solution with and without 1 M methanol. The scan rate was set as 0.1 mV s^{-1} to minimize the interference of the double layer as much as possible. The Tafel slope was calculated from the following equation: $\eta = a +$

b log (j). The electrochemical impedance spectroscopy (EIS) was recorded at the frequency ranging from 100 kHz to 50 mHz at 1.53 V vs. RHE with 12 points per decade. The sinus amplitude potential signal was 5 mV. The obtained curves were analyzed and fitted by the ZsimpWin computer program. The electrochemical surface area (ECSA) was evaluated in terms of double-layer capacitance (C_{dl}) by testing cyclic voltammetry (CV) in a non-Faradaic potential region ranging from 1.03 to 1.13 V vs. RHE at scan rates of 0.4, 0.6, 0.8, and 1 mV s^{-1}. The C_{dl} was estimated by plotting the $\Delta j = (ja - jc)/2$ against the scan rate, the slope of the fitting line represents the C_{dl} (in mF cm^{-2}). ja and jc is the current density at 1.08 V vs. RHE of the positive and negative scans of the CV curves, respectively. The ECSA was calculated from C_{dl} by the equation: $ECSA = C_{dl}/C_s$, where the C_s is the specific capacitance (C_s = 0.04 mF/cm^2, based on typical value reported for metal foam in 1 M KOH aqueous solution).[1]

The SMOR-assisted water splitting was measured in a two-electrode system with the NCS/CF as both anode and cathode electrode. The linear scan voltammetry (LSV) curves were tested at a scan rate of 0.1 mV s^{-1} with the cell voltage ranging from 1.0 V to 1.8 V in 1 M KOH solution with and without 1 M methanol. The CP curve was recorded at a fixed current density of 100 mA cm^{-2} for continuous 100 h. Due to the consumption of methanol during the test, the electrolyte was refreshed every 20 h.

3. Density functional theory (DFT) calculation method

All the calculations were performed in the framework of the density functional theory with the projector augmented plane-wave method, as implemented in the Vienna ab initio simulation package.[2] The generalized gradient approximation proposed by Perdew-Burke-Ernzerhof (PBE) was selected for the exchange-correlation potential.[3] The cut-off energy for the plane wave was set to 480 eV. The energy criterion was set to 10^{-5} eV in the iterative solution of the Kohn-Sham equation. The electronic energy was considered self-consistent when the energy change was smaller than 10^{-5} eV. Geometrical optimization was considered convergent when the energy change was smaller than 0.05 eV/A. The Brillourin zone was sampled with a gamma-centered grid 2×2×1 for $NiCoSe_4$ and NiCo-LDH. We constructed a $NiCoSe_4$ (210) surface with p

(1×1) periodicity in the x and y directions and a NiCo-LDH (107) surface with p (1×1) periodicity in the x and y directions. In the z-direction, a vacuum spacing of 20 Å was applied to separate the surface slab from its periodic duplicates. Here, we defined $\Delta\rho = \rho_{A+B} - \rho_A - \rho_B$ as the charge density difference of A/B heterostructure, where, ρ_{A+B}, ρ_A, and ρ_B were the charge densities of A/B heterostructure, isolated A and B slabs, respectively. We used the Bader charge to express the charge transfer quantity.

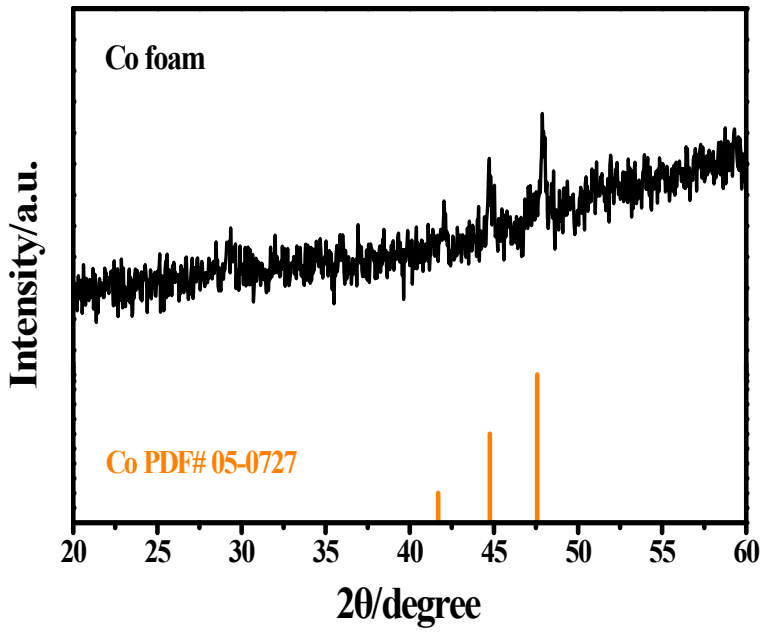

Fig. S1. XRD pattern of the cleaned Co foam.

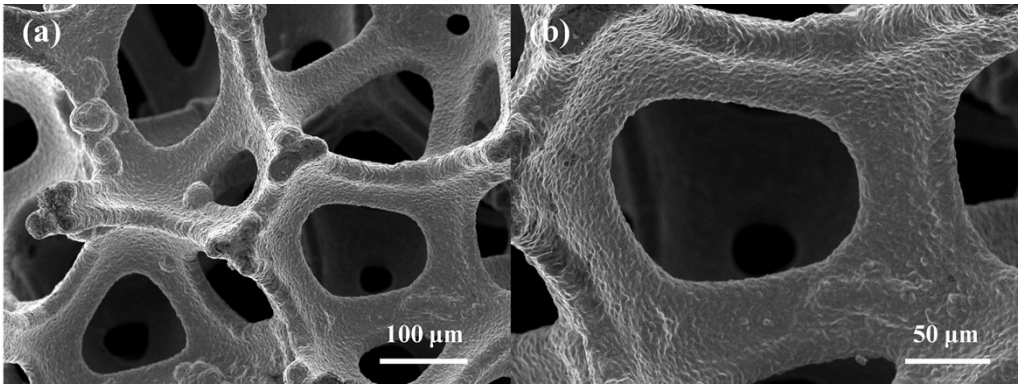

Fig. S2. SEM images of the cleaned CF.

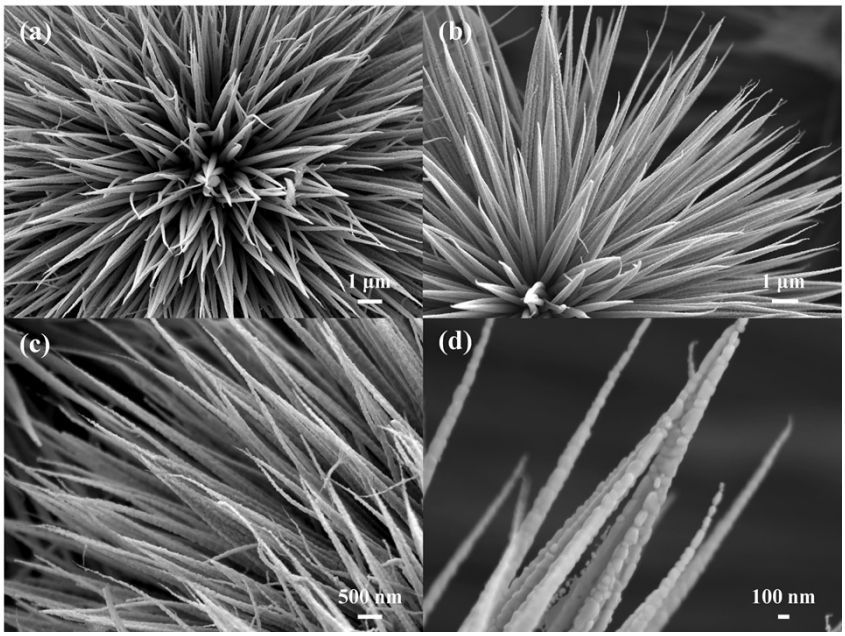

Fig. S3. SEM images of CS/CF.

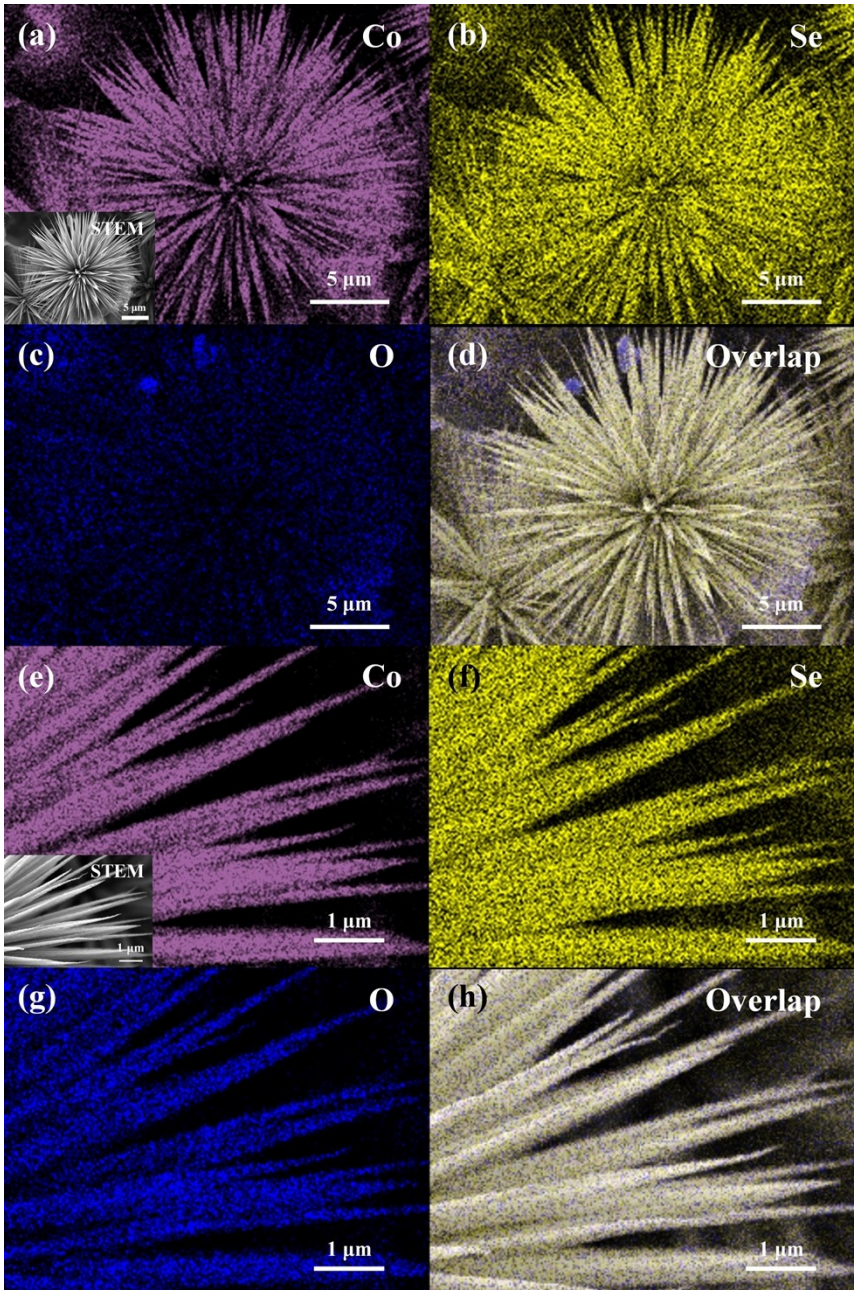

Fig. S4. STEM and elemental mapping images of CS/CF.

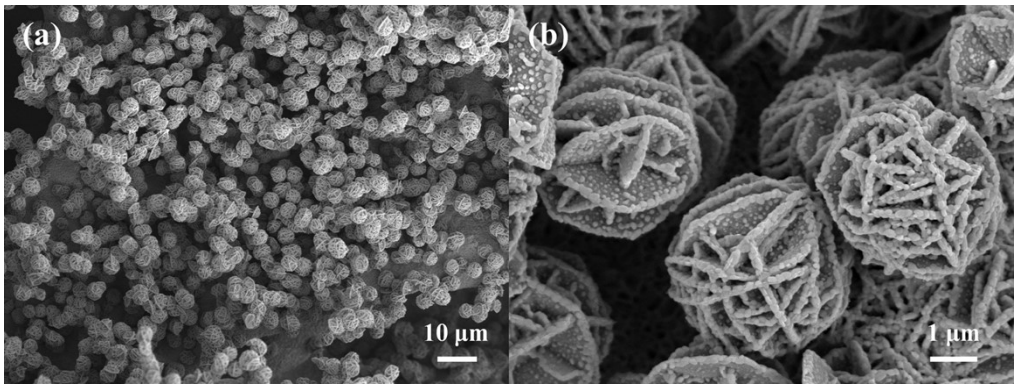

Fig. S5. SEM images of NS/CF.

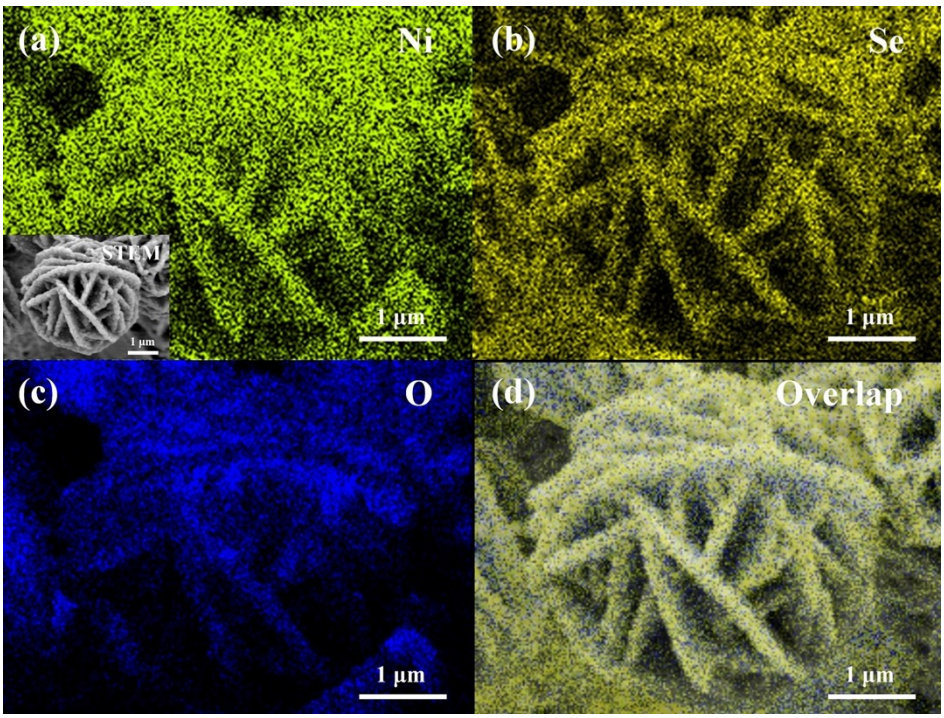

Fig. S6. STEM and elemental mapping images of NS/CF.

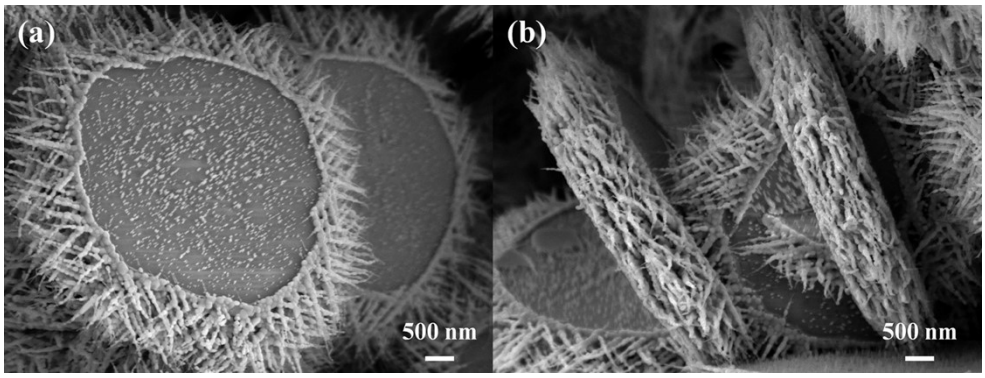

Fig. S7. SEM images of NCS/CF.

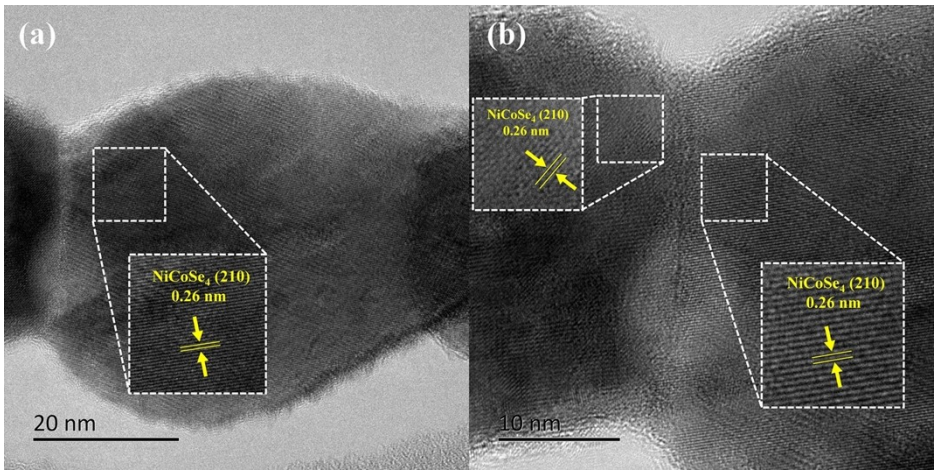

Fig. S8. HRTEM images of $NiCoSe_4$ nanoneedles.

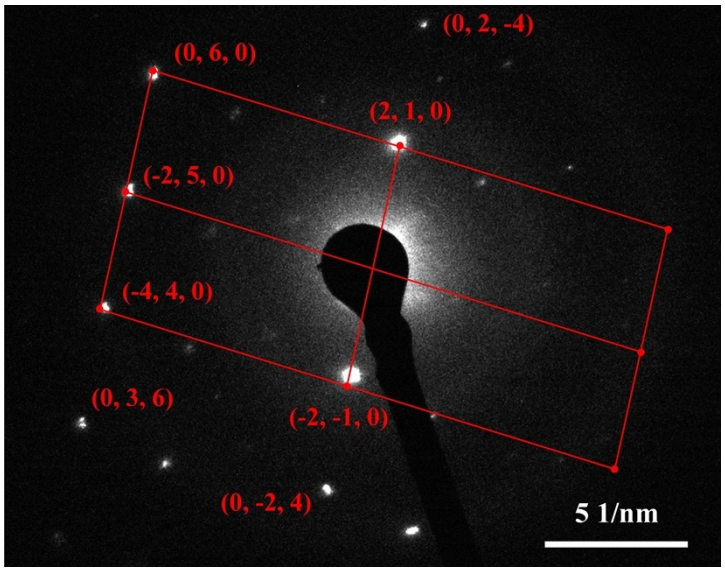

Fig. S9. SAED pattern of $NiCoSe_4$ nanoneedles.

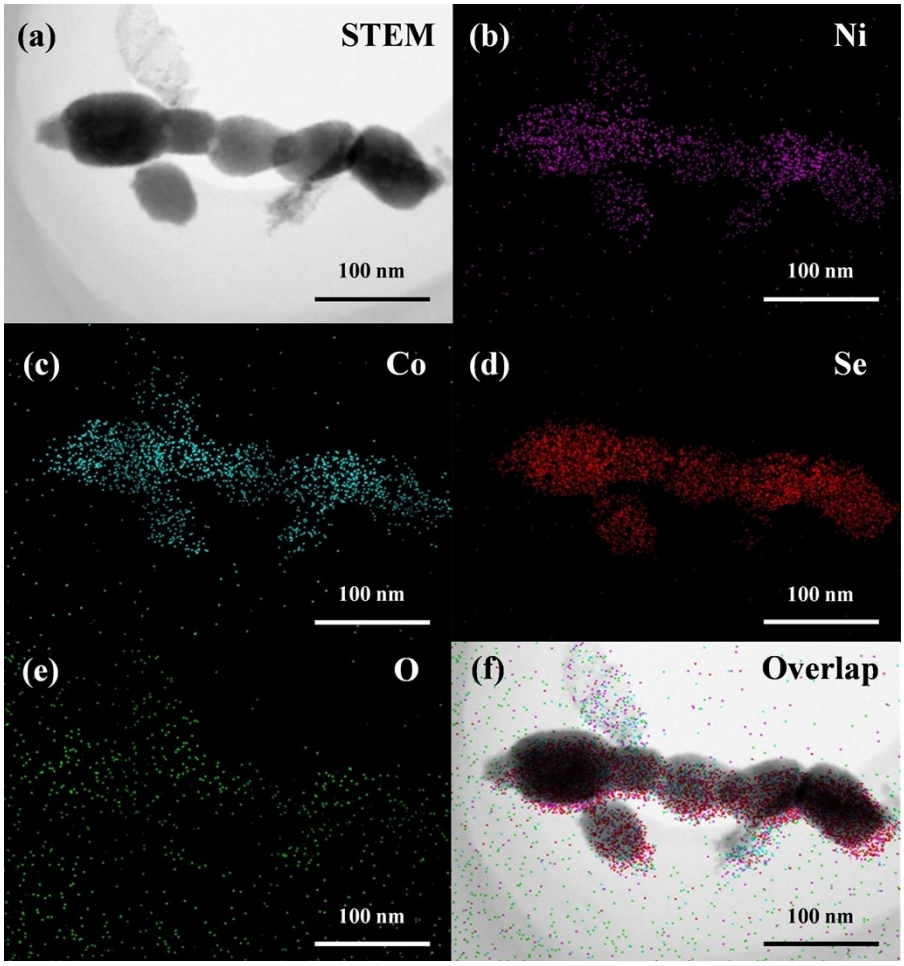

Fig. S10. STEM and elemental mapping images of $NiCoSe_4$ nanoneedles.

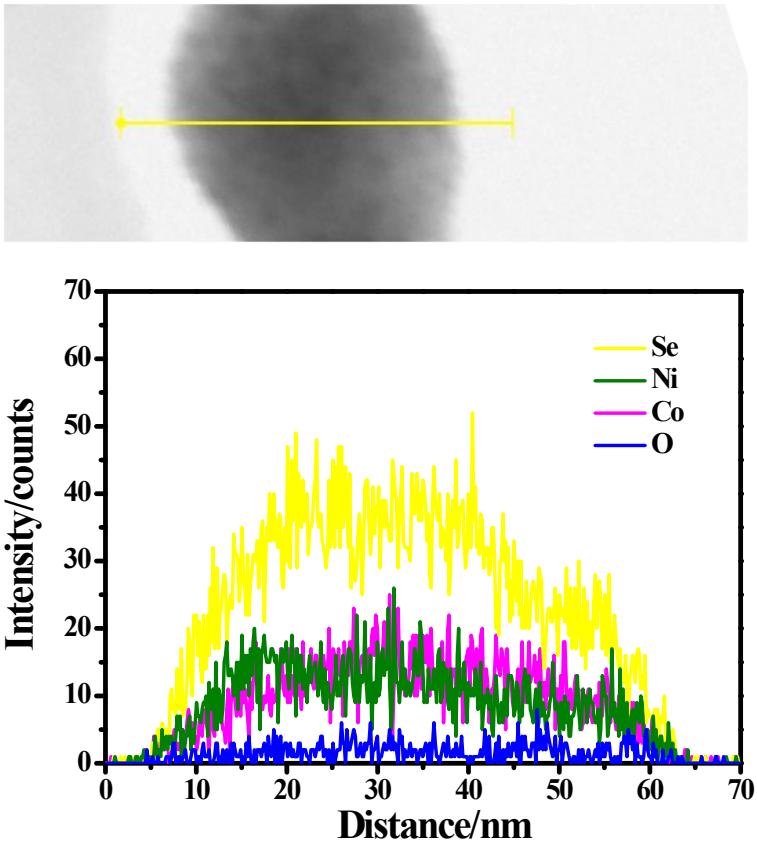

Fig. S11. EDS line scan images of $NiCoSe_4$ nanoneedles.

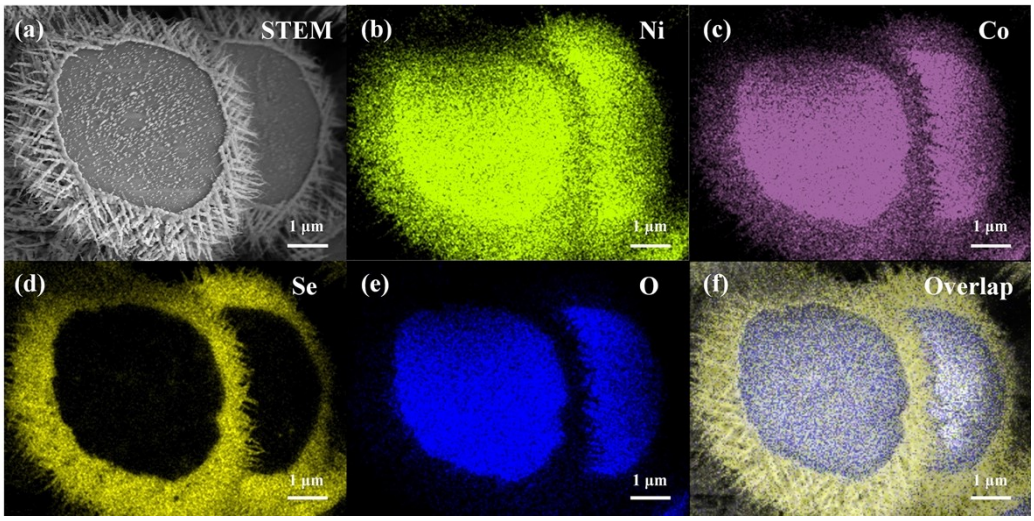

Fig. S12. STEM and elemental mapping images of NCS/CF.

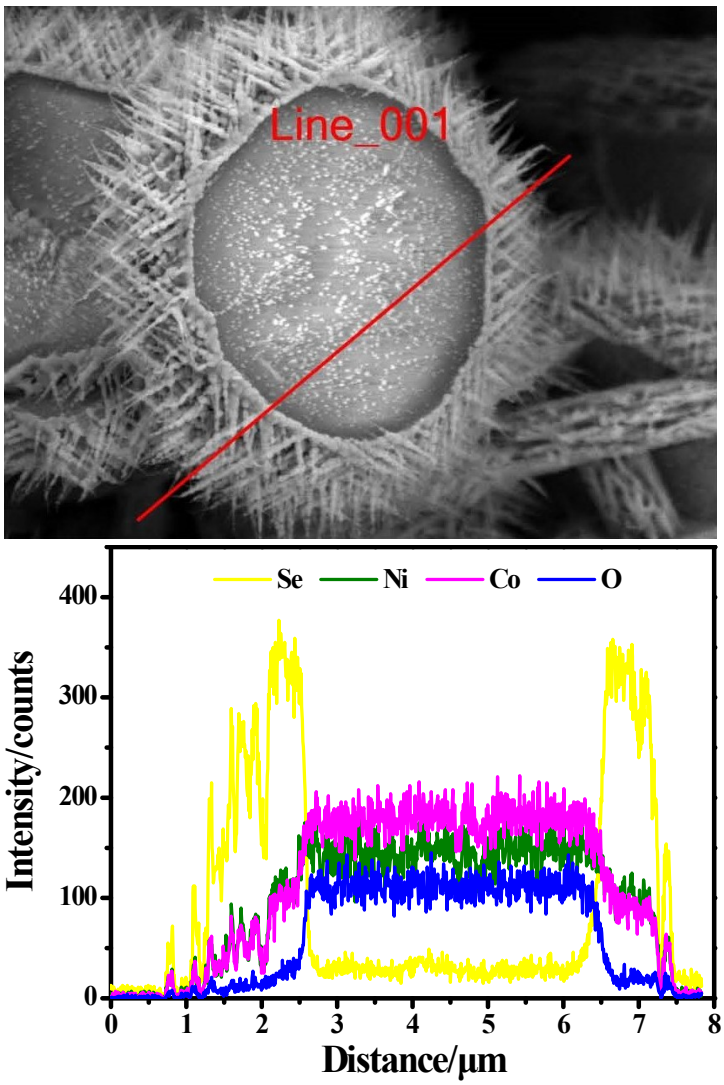

Fig. S13. EDS line scan images of NCS/CF.

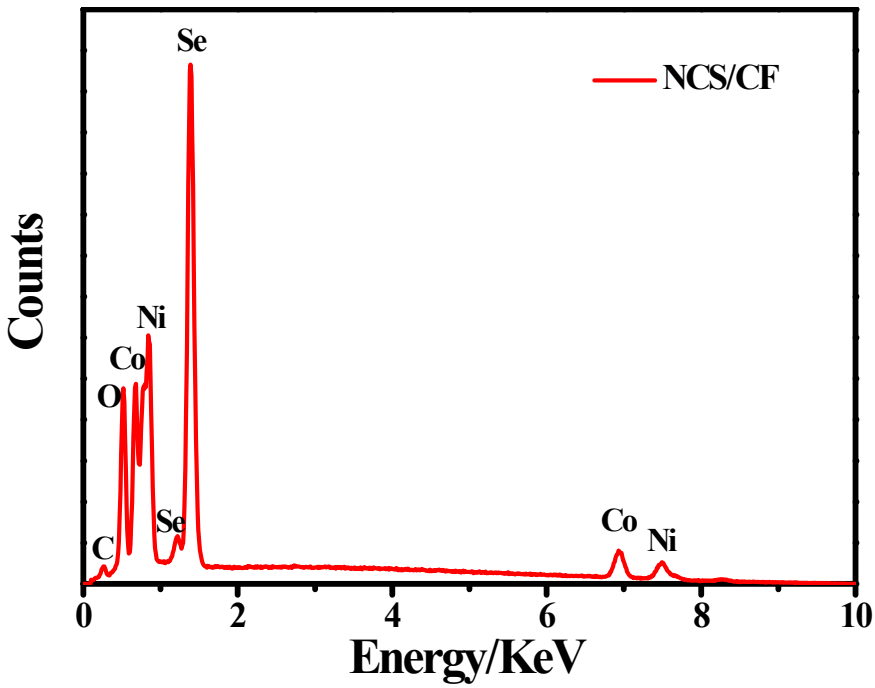

Fig. S14. EDS pattern of NCS/CF.

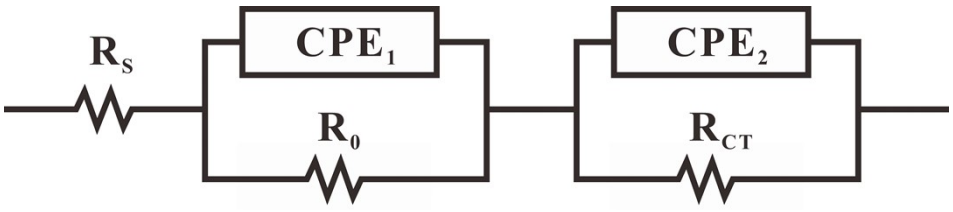

Fig. S15. The equivalent circuit used in EIS fitting.

R_s is a sign of the uncompensated solution resistance, R_{ct} is a charge transfer resistance arising from SMOR, R_0 is associated with the contact resistance, and the constant phase element (CPE_1 and CPE_2) corresponds to the double layer capacitance.

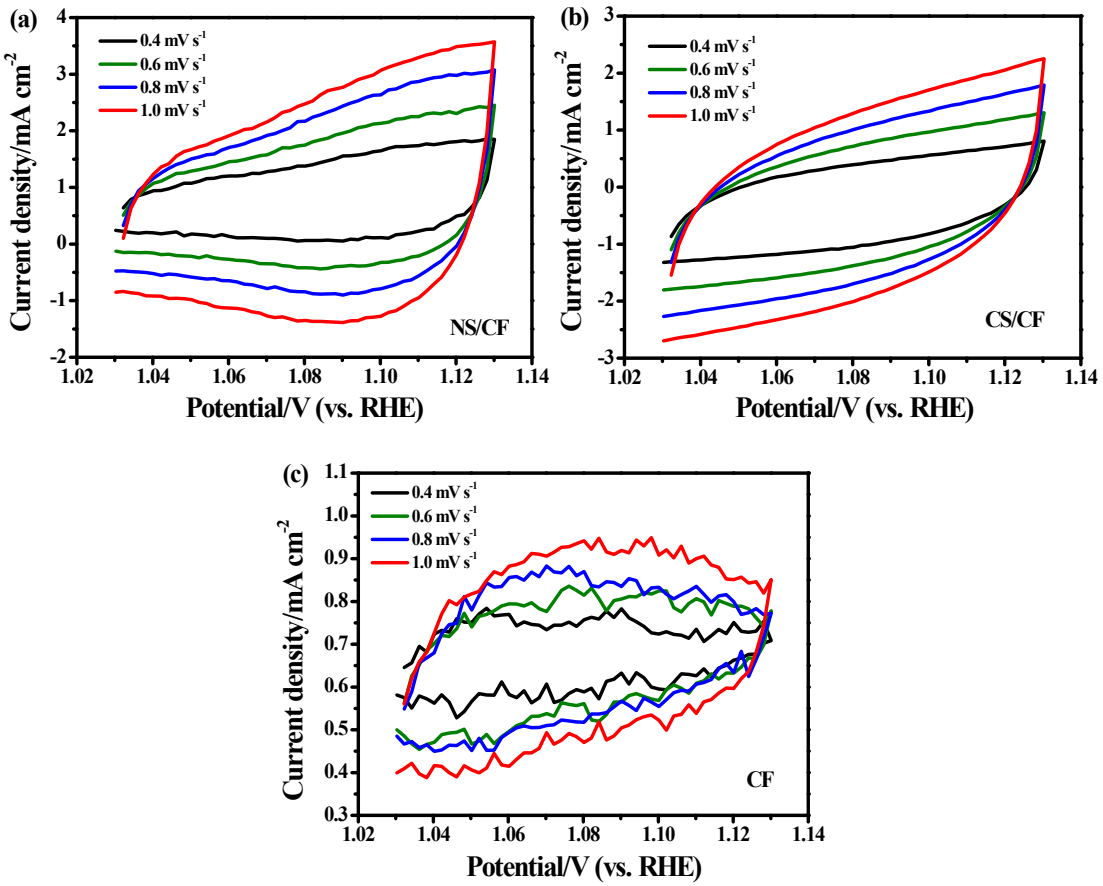

Fig. S16. Non-Faradaic CV curves at different scan rates of 0.4, 0.6, 0.8, and 1.0 mV s^{-1} for (a) NS/CF, (b) CS/CF, and (c) CF.

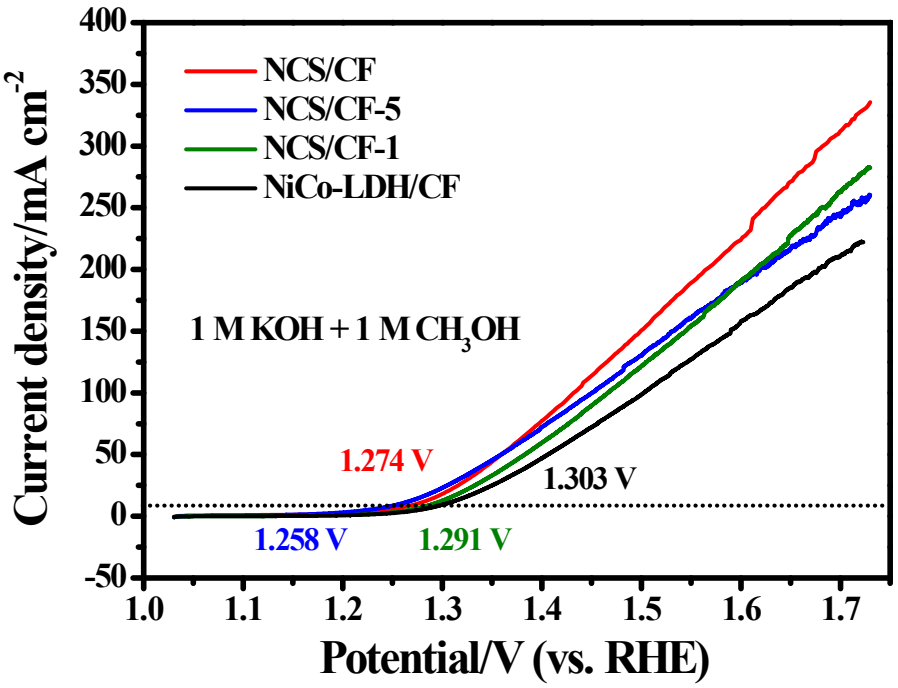

Fig. S17. The activity comparison of NCS/CF-1, NCS/CF, NCS/CF-5, and NiCo-LDH/CF.

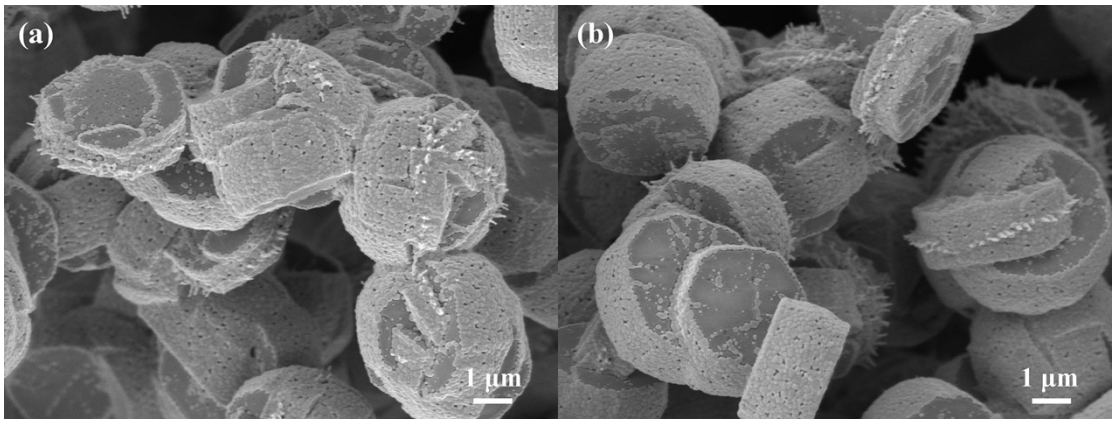

Fig. S18. SEM images of NCS/CF-1.

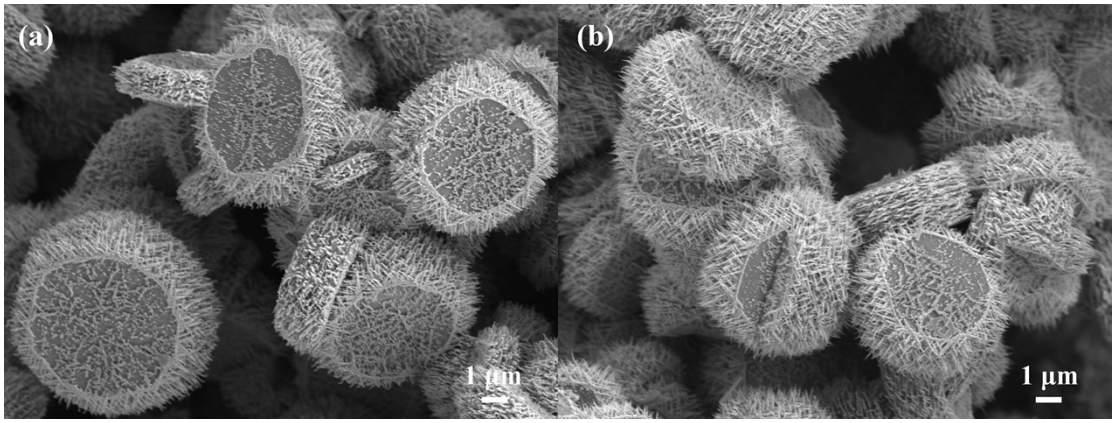

Fig. S19. SEM images of NCS/CF-5.

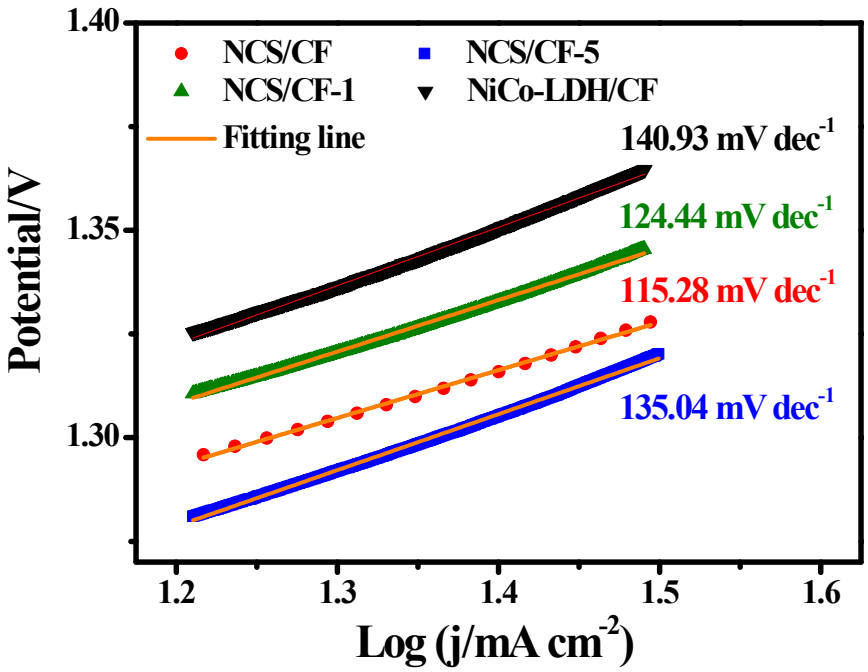

Fig. S20. Tafel slop of NCS/CF-1, NCS/CF, NCS/CF-5, and NiCo-LDH/CF.

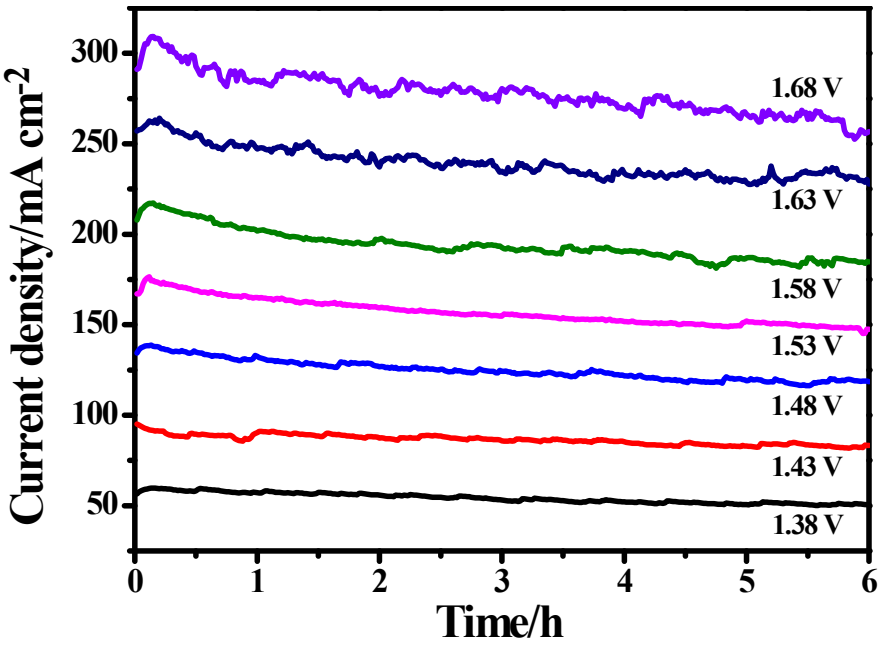

Fig. S21. CA curves of NCS/CF at different potential of 1.38, 1.43, 1.48, 1.53, 1.58, 1.63, and 1.68 V vs. RHE.

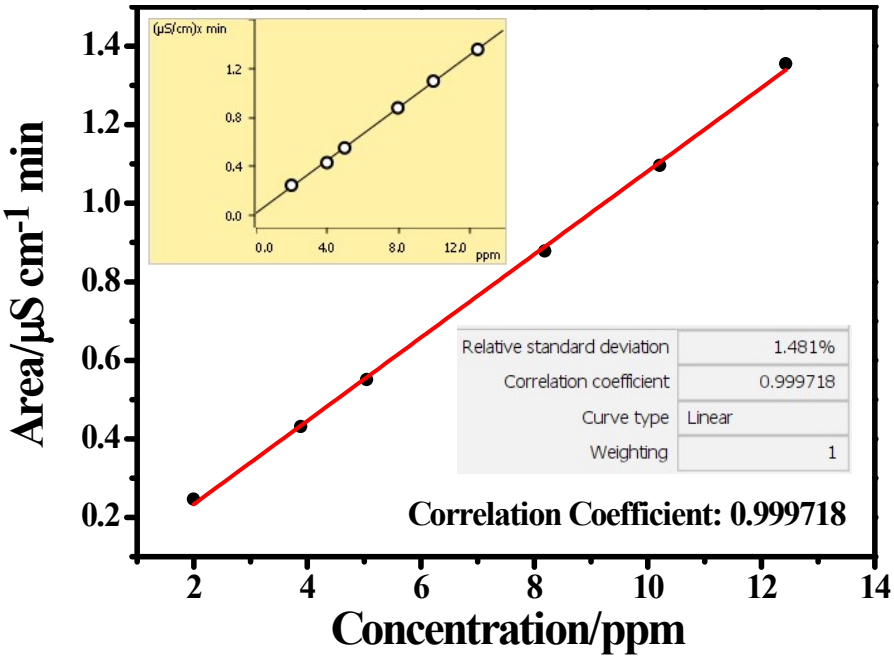

Fig. S22. The calibration curve of IC made by chromatographic grade formate.

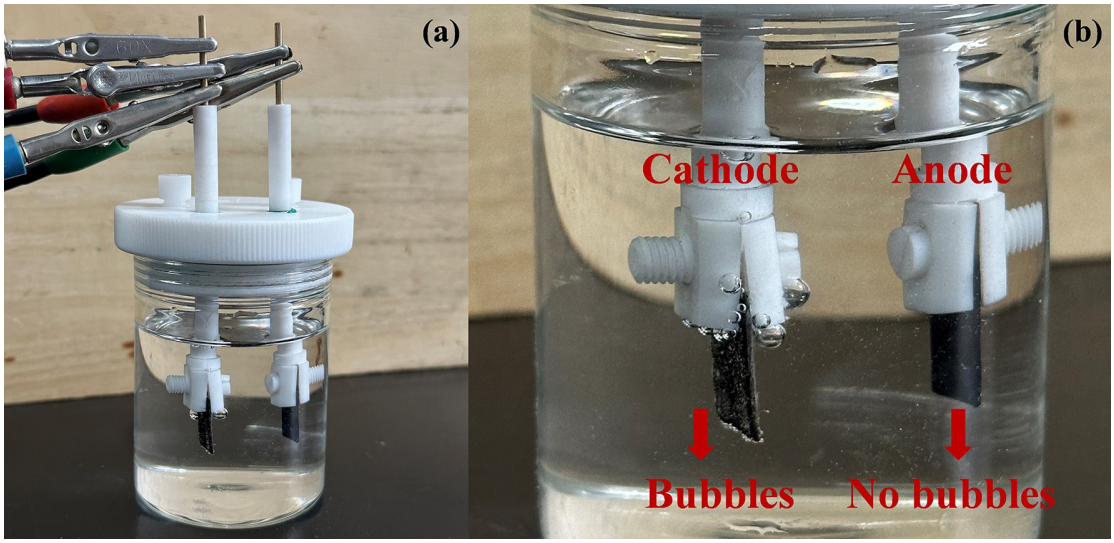

Fig. S23. The digital photograph of NCS/CF||NCS/CF electrolytic cell.

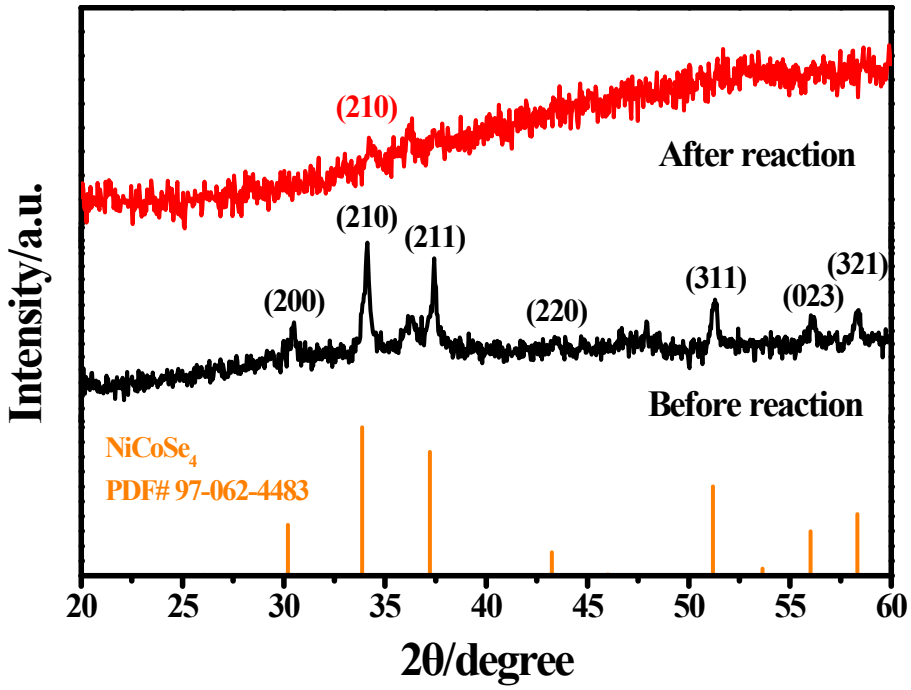

Fig. S24. XRD pattern of NCS/CF after SMOR reaction.

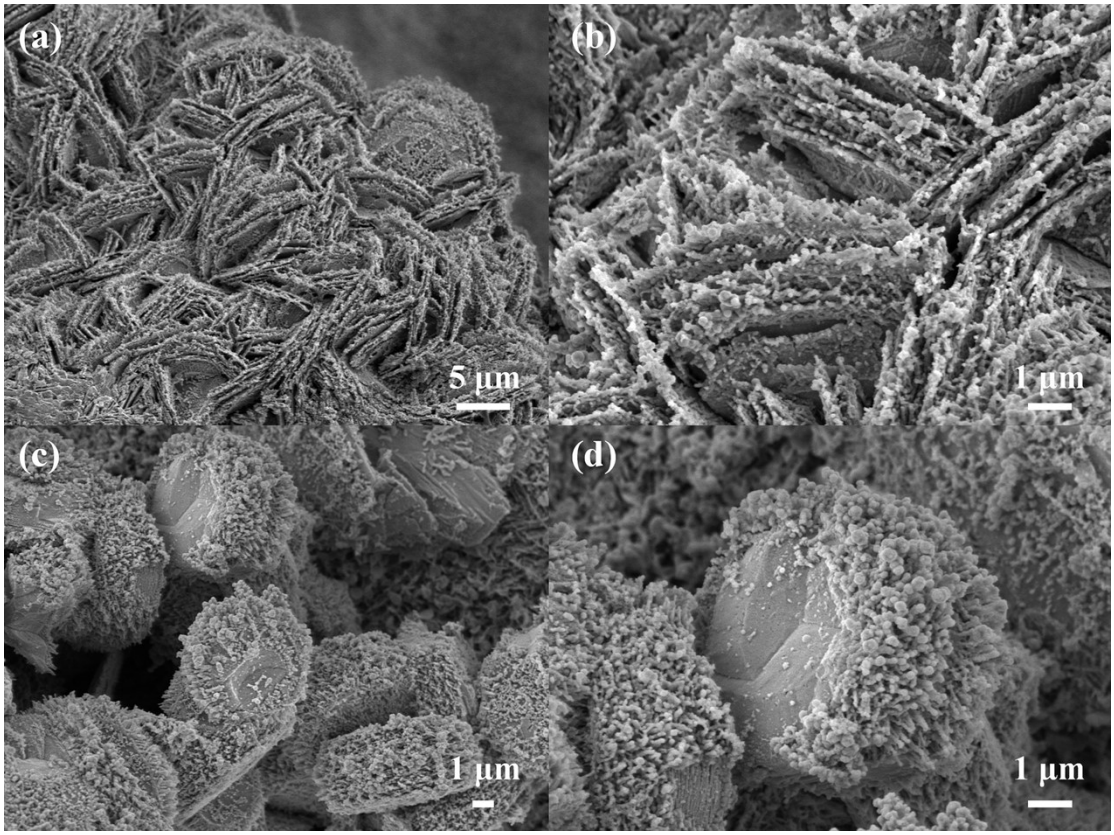

Fig. S25. SEM images of NCS/CF after SMOR reaction.

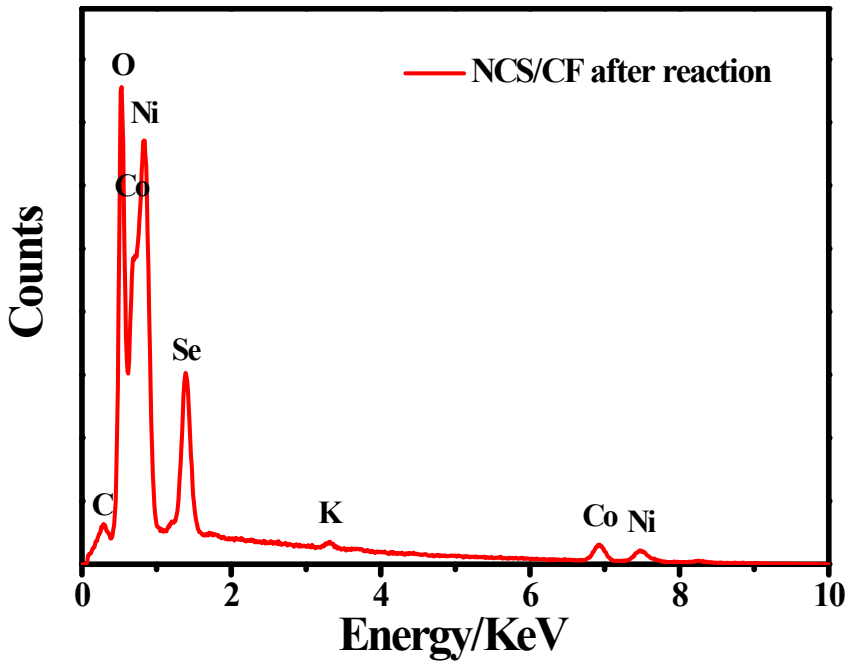

Fig. S26. EDS pattern of NCS/CF after SMOR reaction.

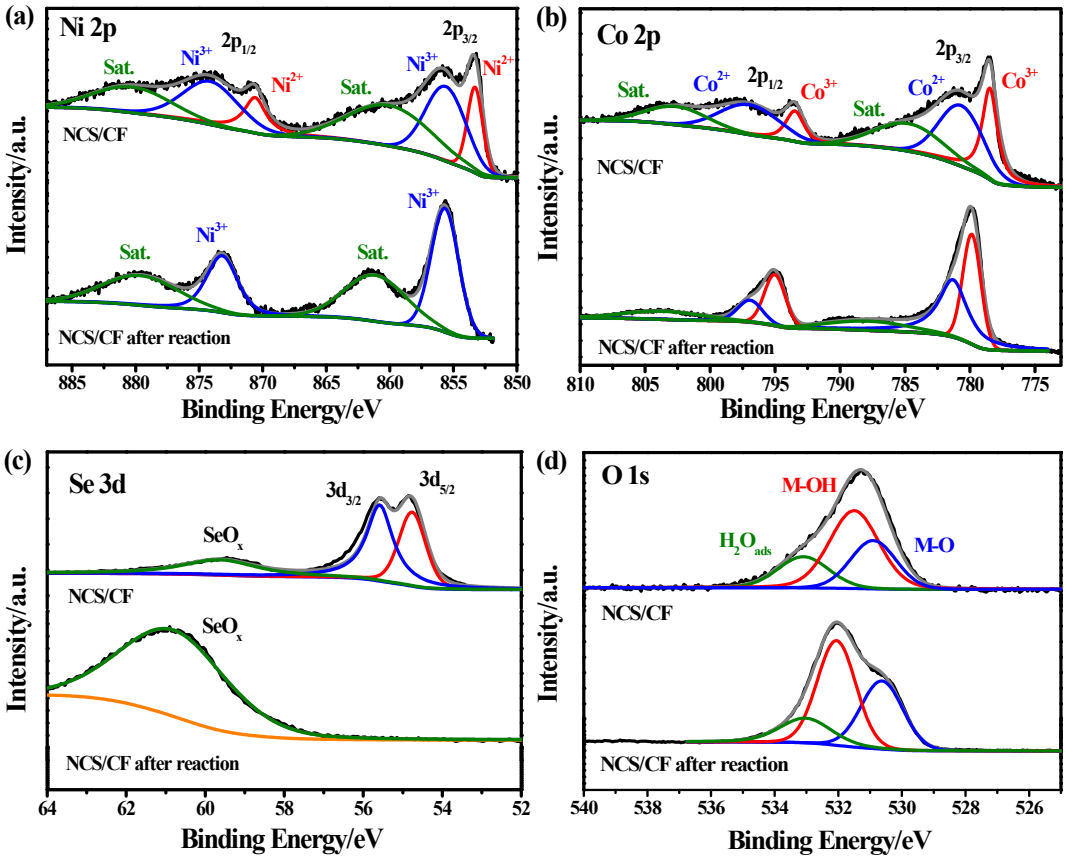

Fig. S27 XPS spectra of Ni 2p region (a), Co 2p region (b), Se 3d region (c), and O 1s region (d) for NCS/CF after SMOR reaction.

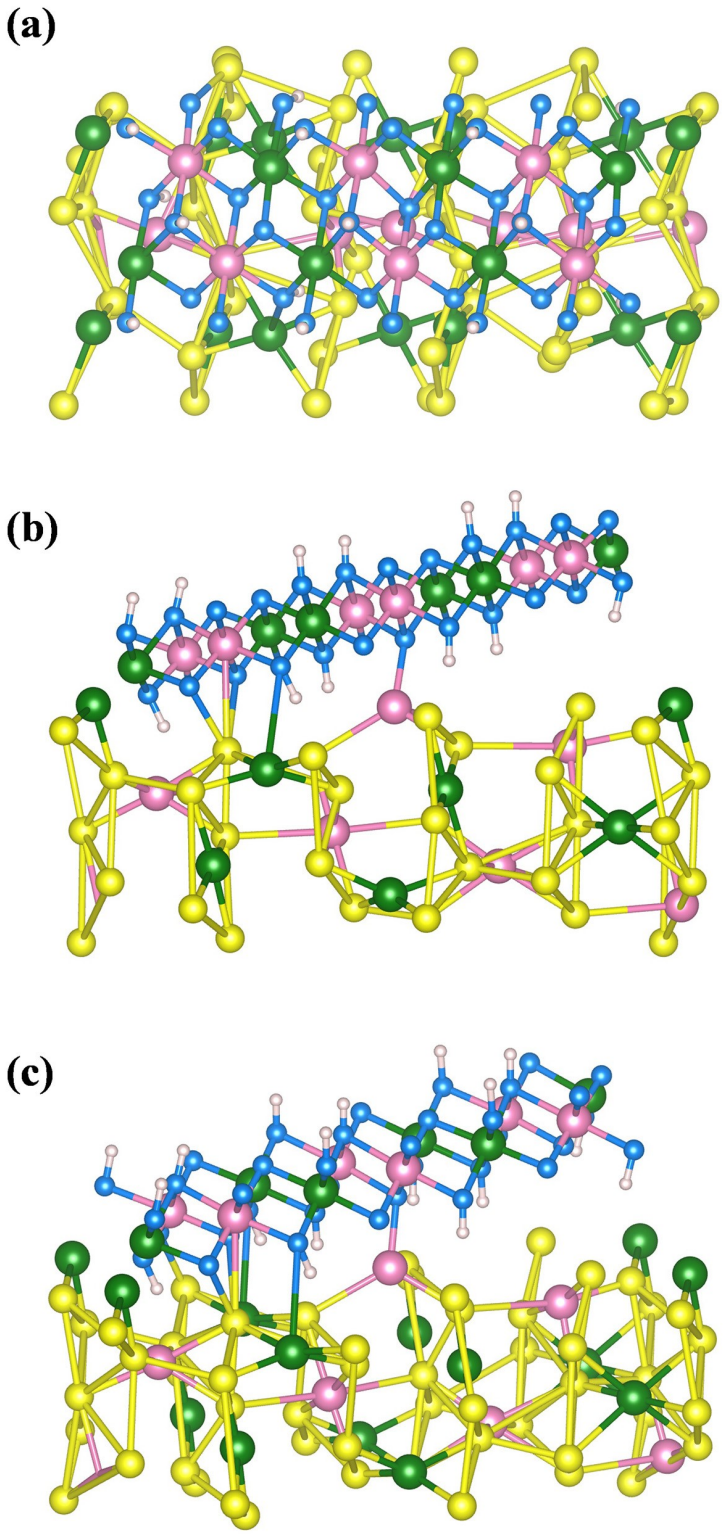

Fig. S28. The (a) front view, (b) side view, and (c) 3D view of the structural model of NCS.

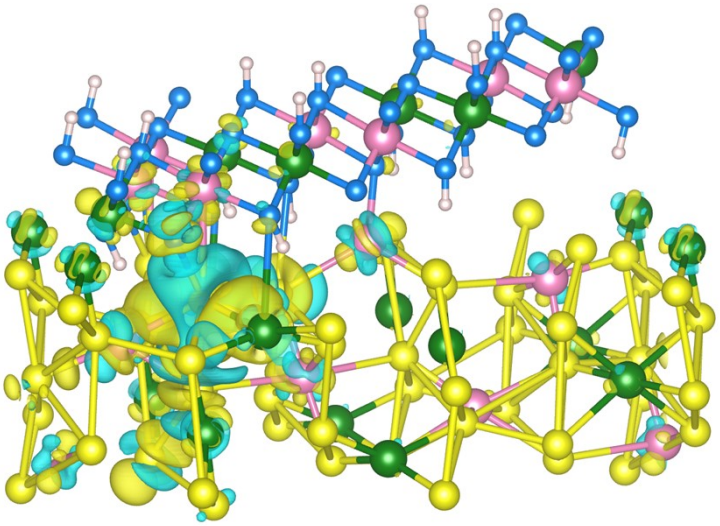

Fig. S29. The differential charge density of NCS.

Table S1. Element composition of NCS/CF based on the EDS.

Element	Weight %	Atomic %
Ni	19.02	17.05
Co	18.30	16.34
Se	53.59	35.71
O	8.16	26.83
C	0.93	4.07

Table S2. The binding energy of Ni 2p for NCS/CF and NS/CF.

Catalysts	Binding energy/eV					
	Ni $2p_{3/2}$			Ni $2p_{1/2}$		
	Ni^{2+}	Ni^{3+}	Satellite	Ni^{2+}	Ni^{3+}	Satellite
NS/CF	853.04	855.48	860.74	870.34	873.91	880.51
NCS/CF	853.29	855.59	860.08	870.59	874.13	880.27

Table S3. The binding energy of Co 2p for NCS/CF and CS/CF.

Catalysts	Binding energy/eV					
	Co $2p_{3/2}$			Co $2p_{1/2}$		
	Co^{3+}	Co^{2+}	Satellite	Co^{3+}	Co^{2+}	Satellite
CS/CF	778.64	780.71	784.58	793.64	797.00	802.35
NCS/CF	778.47	780.68	784.72	793.47	796.98	802.63

Table S4. The binding energy of Se 3d for NCS/CF, NS/CF, and CS/CF.

Catalysts	Binding energy/eV		
	Se-O	Se $3d_{3/2}$	Se $3d_{5/2}$
CS/CF	59.71	55.62	54.86
NS/CF	59.00	55.35	54.51
NCS/CF	59.62	55.58	54.76

Table S5. The catalytic performance of the catalysts for SMOR and SMOR&HER in literatures.

Catalyst	Electrolyte	Scan rate /mV s^{-1}	Potential at a certain current density for SMOR/V vs. RHE	Faradaic efficiency of formate/%	Potential at 10 mA cm^{-2} for SMOR&HER/V vs. RHE	Stability/ h	Ref.
$NiCo_xP$@ NiCo-LDH/CC	1 M KOH + 0.5 M CH_3OH	5	1.23@10 mA cm^{-2}	~100	1.43@10 mA cm^{-2}	20@50 mA cm^{-2}	4
Co_xP@NiCo-LDH	1 M KOH + 0.5 M CH_3OH	5	1.24@10 mA cm^{-2}	~100	1.43@10 mA cm^{-2}	20@40 mA cm^{-2}	5
NCS/CF	**1 M KOH + 1 M CH_3OH**	**0.1**	**1.274@10 mA cm^{-2} 1.432@100 mA cm^{-2}**	**~100**	**1.38@10 mA cm^{-2}**	**100@100 mA cm^{-2}**	**This work**
$Cu_{0.33}$CoCo-LDH/CF	1 M KOH + 3 M CH_3OH	/	1.28@10 mA cm^{-2}	~100	/	24@20 mA cm^{-2}	6
Co_3O_{4-x}/NF-P	1 M KOH + 1 M CH_3OH	/	1.318@10 mA cm^{-2}	>95	1.54@10 mA cm^{-2}	25@100 mA cm^{-2}	7
NiCu@Cu	1 M KOH + 2 M CH_3OH	5	1.32@10 mA cm^{-2}	/	1.45@10 mA cm^{-2}	18@10 mA cm^{-2}	8
FeRu-MOF	1 M KOH + 4 M CH_3OH	5	1.32@10 mA cm^{-2}	>90	1.40@10 mA cm^{-2}	24@20 mA cm^{-2}	9
Fe_2O_3/NiO-NF	1 M KOH + 1 M CH_3OH	5	1.328 onset 1.654@500 mA cm^{-2}	>98	/	/	10
NiIr-MOF/NF	1 M KOH + 4 M CH_3OH	5	1.33@10 mA cm^{-2} 1.41@100 mA cm^{-2}	~100	1.39@10 mA cm^{-2}	20@10 mA cm^{-2}	11
$Ni_{0.33}Co_{0.67}(OH)_2$/NF	1 M KOH +	5	1.33@10 mA cm^{-2}	~100	1.5@10 mA cm^{-2}	12@20	12

	0.5 M CH_3OH					mA cm^{-2}	
Cu_3N	1 M KOH + 1 M CH_3OH	/	1.35@10 mA cm^{-2}	>90	/	/	13
Ni-MOFs-120/NF	1 M KOH + 0.5 M CH_3OH	5	1.37@10 mA cm^{-2} 1.44@100 mA cm^{-2}	/	/	/	14
Cu_2Se/Co_3Se_4	1 M KOH + 1 M CH_3OH	5	1.39@10 mA cm^{-2}	100	/	/	15
NiFe LDH@SnO_2/NF	1 M KOH + 0.5 M CH_3OH	5	1.396@10 mA cm^{-2}	/	/	/	16
β-$Ni(OH)_2$/NF	1 M KOH + 1 M CH_3OH	5	1.398@10 mA cm^{-2}	99.98	1.684@10 mA cm^{-2}	/	17
NiFe-LDH/NiFe-HAB/CF	1 M KOH + 3 M CH_3OH	/	1.416@10 mA cm^{-2} 1.538@100 mA cm^{-2}	~100	/	/	18
Ni_3S_2-CNFs	1 M KOH + 1 M CH_3OH	5	1.40@100 mA cm^{-2}	99.82	/	/	19
CC@$NiCo_2S_4$	1 M KOH + 1 M CH_3OH	5	1.40@100 mA cm^{-2}	~100	1.32@10 mA cm^{-2}	12@100 mA cm^{-2}	20
FCNS@NF	1 M KOH + 1 M CH_3OH	2	1.42@100 mA cm^{-2}	98.67	/	/	21
Nb_2O_5/NF	1 M KOH + 1 M CH_3OH	/	1.47@100 mA cm^{-2}	~100	/	/	22
NiO/NF	1 M KOH + 1 M CH_3OH	10	1.53@100 mA cm^{-2}	/	/	/	23
h-NiSe/CNTs	1 M KOH + 1 M CH_3OH	5	1.66@100 mA cm^{-2}	97.97	/	/	24

Table S6. The catalytic performance of the catalysts for OER in literatures.

Catalyst	Electrolyte	Scan rate /mV s^{-1}	Overpotential at 10 mA cm^{-2}/V vs. RHE	Ref.
O-MoNi-C/NF	1 M KOH	/	190	[25]
Ag_{SA}-NiCo LDH/CC	1 M KOH	5	192	[26]
CeO_x-$NiCo_2O_4$-U/NF	1 M KOH	5	219	[27]
N-NiCoFe	1 M KOH	2	220	[28]
NiFe LDH/Ni-NWN	1 M KOH	1	222	[29]
C-$CoSe_2$	1 M KOH	5	227	[30]
NCS/CF	**1 M KOH**	**0.1**	**227**	**This work**
CeO_x@$NiCo_2O_4$/NF	1 M KOH	/	238	[31]
5.0 Mn-NiFe LDH/rGO	1 M KOH	5	240	[32]
NiCo-NR	1 M KOH	5	244	[33]
NiCo@Ni_3S_2/NF	1 M KOH	5	245	[34]
Ni NDC-Co/CP	1 M KOH	5	245	[35]
Mo-CoOOH	1 M KOH	5	249	[36]
NiCo-LDH/CoP/NF	1 M KOH	50	253	[37]
$NiSe_2$@Fe–NiCo LDH	1 M KOH	5	260	[38]
NiCo@rGO	1 M KOH	10	261	[39]
$NiCoO_2$@NiCo LDH	1 M KOH	1	272	[40]
0.5Mo-$NiCo_2O_4$	3 M KOH	5	280	[41]
$MoCo(OH)_2$/CoP/NF	1 M KOH	1	287	[42]

Table S7. EIS fitting parameters from equivalent circuit of the catalysts for SMOR.

Catalysts	R_s / Ω	CPE / S s^{-n}	n / 0<n<1	R_{ct} / Ω	CPE / S s^{-n}	n / 0<n<1	R_0 / Ω
CF	0.98	5.344E-002	0.61	32.52	2.039E-002	0.98	7.99
CS/CF	1.00	6.780E-001	0.51	1.30	1.679E-000	0.77	0.33
NS/CF	1.06	3.906E-001	0.50	0.74	1.570E-000	0.64	0.16
NCS/CF	0.99	1.428E-000	0.35	0.49	6.456E-000	1.00	0.09

Table S8. Element composition of NCS/CF based on the EDS after SMOR reaction.

Element	Weight %	Atomic %
Ni	35.24	24.52
Co	29.40	20.38
Se	16.75	8.67
O	17.88	45.67
K	0.73	0.77

Table S9. The Bader charges of Ni and Co atoms in the NCS model.

Atom	Number	Bader charge
Ni	1	0.56
Ni	2	0.36
Ni	3	0.39
Ni	4	0.35
Ni	5	0.38
Ni	6	0.40
Ni	7	1.29
Ni	8	1.23
Ni	9	1.26
Ni	10	1.26
Ni	11	1.27
Ni	12	1.33
Total Bader charge		**10.09**
Co	1	0.47
Co	2	0.31
Co	3	0.32
Co	4	0.32
Co	5	0.39
Co	6	0.32
Co	7	0.87
Co	8	1.20
Co	9	1.22
Co	10	1.22
Co	11	1.16
Co	12	1.06
Total Bader charge		**8.87**

Positive/negative value corresponds to loss/gain of electron.[43]

Table S10. The Bader charges of Se atoms in the NCS model.

Atom	Number	Bader charge
Se	1	-0.13
Se	2	-0.12
Se	3	-0.18
Se	4	-0.15
Se	5	-0.27
Se	6	-0.24
Se	7	-0.21
Se	8	-0.18
Se	9	-0.13
Se	10	-0.19
Se	11	-0.28
Se	12	-0.12
Se	13	-0.33
Se	14	-0.16
Se	15	-0.16
Se	16	-0.27
Se	17	-0.02
Se	18	-0.19
Se	19	0.06
Se	20	-0.11
Se	21	-0.16
Se	22	-0.18
Se	23	-0.07
Se	24	-0.15
Total Bader charge		**-3.95**

Positive/negative value corresponds to loss/gain of electron.[43]

References

1. D. Liu, H. Ai, J. Li, M. Fang, M. Chen, D. Liu, X. Du, P. Zhou, F. Li, K. H. Lo, Y. Tang, S. Chen, L. Wang, G. Xing and H. Pan, *Adv. Energy Mater.*, 2020, **10**, 2002464.
2. G. Kresse and D. Joubert, *Phys. Rev. B*, 1999, **59**, 1758-1775.
3. J. P. Perdew, K. Burke and M. Ernzerhof, *Phys. Rev. Lett.*, 1996, **77**, 3865-3868.
4. Y. Zhang, X. Wu, G. Fu, X. Fu and J. Luo, *J. Alloy. Compd.*, 2022, **906**, 164305.
5. M. Li, X. Deng, Y. Liang, K. Xiang, D. Wu, B. Zhao, H. Yang, J.-L. Luo and X.-Z. Fu, *J. Energy Chem.*, 2020, **50**, 314-323.
6. B. Liu, T. Xiao, X. Sun, H.-Q. Peng, X. Wang, Y. Zhao, W. Zhang and Y.-F. Song, *J. Mater. Chem. A*, 2022, **10**, 19649-19661.
7. J. Zhang, Y. Hua, H. Li, X. Zhang, C. Shi, Y. Li, L. Di and Z. Wang, *Chem. Eng. J.*, 2023, **478**, 147288.
8. F. Arshad, A. Tahir, T. u. Haq, H. Duran, I. Hussain and F. Sher, *Int. J. Hydrogen Energy*, 2022, **47**, 36118-36128.
9. Q. Ling, Z. Zhao, Z. Li, K. Yan, C. Ding, P. Chen, Z. Sun, G. He, J. Lv and M. Zhang, *J. Mater. Chem. A*, 2023, **11**, 2876-2888.
10. Y. Hao, D. Yu, S. Zhu, C. Kuo, Y. Chang, L. Wang, H. Chen, M. Shao and S. Peng, *Energ. Environ. Sci*, 2023, **16**, 1100-1110.
11. Y. Xu, M. Liu, M. Wang, T. Ren, K. Ren, Z. Wang, X. Li, L. Wang and H. Wang, *Appl. Catal. B.*, 2022, **300**, 120753.
12. M. Li, X. Deng, K. Xiang, Y. Liang, B. Zhao, J. Hao, J. Luo and X. Fu, *ChemSusChem*, 2020, **13**, 914-921.
13. L. Zhao, Q. Sun, M. Li, Y. Zhong, P. Shen, Y. Lin and K. Xu, *Sci. China Mater.*, 2023, **66**, 1820-1828.
14. J. Li, *Electrochem. Commun.*, 2023, **146**, 107416.
15. B. Zhao, J. Liu, C. Xu, R. Feng, P. Sui, J.-X. Luo, L. Wang, J. Zhang, J.-L. Luo and X.-Z. Fu, *Appl. Catal. B-Environ*, 2021, **285**, 119800.
16. C. Wan, J. Jin, X. Wei, S. Chen, Y. Zhang, T. Zhu and H. Qu, *J. Mater. Sci. Technol.*, 2022, **124**, 102-108.
17. L. Gong, N. Xuan, G. Gu, P. Lv, N. Huang, C. Song, M. Zheng, J. Wang, P. Cui, G. Gu, Y. Jia, G. Cheng and Z. Du, *Nano Energy*, 2023, **107**, 108124.
18. S. Jiang, T. Xiao, C. Xu, S. Wang, H. Peng, W. Zhang, B. Liu and Y. Song, *Small*, 2023, **19**, 2208027.
19. B. Zhao, J. Liu, X. Wang, C. Xu, P. Sui, R. Feng, L. Wang, J. Zhang, J. Luo and X. Fu, *Nano Energy*, 2021, **80**, 105530.
20. F. Si, J. Liu, Y. Zhang, B. Zhao, Y. Liang, X. Wu, X. Kang, X. Yang, J. Zhang, X. Fu and J. Luo, *Small*, 2023, **19**, 2205257.
21. Y. Yi, J. Li and C. Cui, *Chinese Chem. Lett.*, 2022, **33**, 1006-1010.
22. X. Wang, C. Xiao, Y. Li, T. Murayama, T. Ishida, M. Lin and G. Xiu, *Appl. Catal. A-Gen*, 2023, **664**, 119341.
23. M. I. Abdullah, A. Hameed, N. Zhang, M. H. Islam, M. Ma and B. G. Pollet, *ACS Appl. Mater. Inter.*, 2021, **13**, 30603-30613.
24. B. Zhao, J. Liu, C. Xu, R. Feng, P. Sui, L. Wang, J. Zhang, J. Luo and X. Fu, *Adv. Funct. Mater.*, 2021, **31**, 2008812.

25. M. Y. Zu, C. Wang, L. Zhang, L. R. Zheng and H. G. Yang, *Mater. Horiz.*, 2019, **6**, 115-121.
26. W. He, R. Zhang, H. Liu, Q. Hao, Y. Li, X. Zheng, C. Liu, J. Zhang and H. L. Xin, *Small*, 2023, **19**, 2301610.
27. J. Ji, J. Xu, G. Fan, T. Guo, L. Yang and F. Li, *Electrochim. Acta*, 2021, **382**, 138345.
28. P. Wang, Y. Yu, Y. Yan, B. Qin, Z. Ye, W. Zhong, W. Cai and X. Zheng, *J. Alloy. Compd.*, 2023, **941**, 168954.
29. K. M. Amin, K.-H. Lin, M. Duerrschnabel, L. Molina-Luna and W. Ensinger, *ACS Sustain. Chem. Eng.*, 2023, **11**, 15410-15422.
30. S. Zhang, J. Zhang, P. Liang, C. Zhang, T. Kou and Z. Zhang, *J. Power. Sources*, 2021, **497**, 229895.
31. W. Liu, J. Zhao, L. Dai, Y. Qi, K. Liang, J. Bao and Y. Ren, *Inorg. Chem.*, 2024, **63**, 6016-6025.
32. B. Jiang, W.-C. Cheong, R. Tu, K. Sun, S. Liu, K. Wu, H. Shang, A. Huang, M. Wang, L. Zheng, X. Wei and C. Chen, *Sci. China Mater.*, 2021, **64**, 2729-2738.
33. A. Gaur, V. Pundir, R. Kaur, S. N. Jha and V. Bagchi, *ACS Appl. Energ. Mater.*, 2023, **6**, 5360-5367.
34. Y. He, Y. Wang, X. Wang, R. Li and W. Lu, *Int. J. Hydrogen Energy*, 2023, **48**, 35962-35970.
35. H. Yin, X. Liu, L. Wang, T. T. Isimjan, D. Cai and X. Yang, *Inorg. Chem.*, 2024, **63**, 7045-7052.
36. L. Tang, L. Yu, C. Ma, Y. Song, Y. Tu, Y. Zhang, X. Bo and D. Deng, *J. Mater. Chem. A*, 2022, **10**, 6242-6250.
37. Y. Chen, J. He, S. Ye, J. Guan, X. Liu, J. Wang, S. Xu, J. Gu, K. Chen, L. Zhang, B. Lan, R. Cao and H. Liang, *Inorg. Chem. Commun.*, 2023, **157**, 111347.
38. Q. Wang, C. Wang, X. Du and X. Zhang, *Int. J. Hydrogen Energy*, 2024, **51**, 1154-1166.
39. J. Rashid, K. Gilani, A. Arif, C. S. Saraj, W. Li and M. Xu, *Int. J. Hydrogen Energy*, 2024, **51**, 774-786.
40. Z. Wu, X. Hu, C. Cai, Y. Wang, X. Li, J. Wen, B. Li and H. Gong, *J. Colloid Interf. Sci.*, 2024, **657**, 75-82.
41. S. Xiong, L. Wang, H. Chai, Y. Xu, Y. Jiao and J. Chen, *J. Colloid Interf. Sci.*, 2022, **606**, 1695-1706.
42. Y. Xiao, X. Chen, T. Li, Y. Mao, C. Liu, Y. Chen and W. Wang, *Int. J. Hydrogen Energy*, 2022, **47**, 9915-9924.
43. Y. Chen, X. Yan, H. Geng, X. Sheng, L. Zhang, H. Wang, J. Li, Y. Cao and X. Pan, *Inorg. Chem.*, 2021, **60**, 124-129.